Title
Slope-Aspect Induced Climate Differences Influence How Water Is Exchanged Between the Land and Atmosphere

Journal
Journal of Geophysical Research Biogeosciences, 126(5)

ISSN
2169-8953

Authors
Bilir, T Eren
Fung, Inez
Dawson, Todd E

Publication Date
2021-05-01

DOI
10.1029/2020jg006027

Peer reviewed

Slope-aspect induced climate differences influence how water is exchanged between the land and atmosphere

T. Eren Bilir[1], Inez Fung[1,2], Todd E. Dawson[1,3]

[1]UC Berkeley, Department of Environmental Science, Policy, and Management
[2]UC Berkeley, Department of Earth and Planetary Science
[3]UC Berkeley, Department of Integrative Biology

Key Points:

- Solar radiation differences generate different microclimates across adjacent north- and south-facing slopes in the midlatitudes.
- High-frequency measurements document microclimate and covarying tree water use across a hillslope divide over a dry Mediterranean summer.
- Transpiration of a single tree species is higher on the drier, sunnier south-facing slope, suggesting different water use strategies.

Corresponding author: T. Eren Bilir, `tebilir@berkeley.edu`

Abstract

Cross-slope climate differences in the midlatitudes are ecologically important, and impact vegetation-mediated water balance between the earth surface and the atmosphere. We made high-resolution *in situ* observations of air temperature, relative humidity, soil moisture, insolation, and sap velocity observations on 14 Pacific madrone trees (*Arbutus menziesii*) spanning adjacent north and south slopes at the University of California's Angelo Coast Range Reserve. To understand the cross-slope response of sap velocity, a proxy for transpiration, to microclimate, we modeled the sap velocity on each slope using a transpiration model driven by ambient environment and parameterized with a Markov Chain Monte Carlo (MCMC) parameter estimation process. The results show that trees on opposing slopes do not follow a shared pattern of physiological response to transpiration drivers. This means that the observed sap velocity differences are not due entirely to observed microclimate differences, but also due to population-level physiological differences, which indicates acclimation to inhabited microclimate. While our present dataset and analytical tools do not identify mechanisms of acclimation, we speculate that differing proportions of sun-adapted and shade-adapted leaves, differences in stomatal regulation, and cross-slope root zone moisture differences could explain some of the observed and modeled differences.

Plain Language Summary

The transfer of water from plants to the atmosphere is determined by the interaction between plant physiology and local microclimate. We made high-frequency observations of sap velocity in two populations of Pacific madrone trees across a hillslope divide containing a strong microclimatic gradient. The differences in sunlight between the two slopes lead not only to different temperatures and humidities, but also to differences in energy available for photosynthesis, and hence transpiration. As a result, trees on the south-facing slope transpire 20% more water over the dry Mediterranean summer. Furthermore, we found that water use by trees on the north slope bears a different relationship to environmental conditions than water use by trees on the south slope.

1 Introduction

Plant transpiration is a major conduit for the transfer of water from the land to the atmosphere (Jasechko et al., 2013). Recent studies have advanced our understand-

ing of how complex and sensitive the leaf-to-atmosphere link is to localized feedbacks, such as slope exposure and associated conditions (e.g., Link et al. (2014); Harrison et al. (2020); Amitrano et al. (2019)). Microclimates have been highlighted in particular as a distinct control on long-term ecosystem vulnerability, separate from evolving macroclimate (De Frenne et al., 2013, 2019). The urgency of understanding the vulnerability of forest ecosystems to changing climate conditions in arid or Mediterranean climates has been underscored by mass tree die-offs in western North America (Asner et al., 2016; D. J. N. Young et al., 2017; Fettig et al., 2019), and worsening wildfire regimes around the world. Yet, the influence of natural microclimatic variations, such as those associated with topographic position, on plant–water relations and physiology is often omitted in models used to forecast ecosystem vulnerability, due to a lack of data (Pappas et al., 2016; Mencuccini et al., 2019).

Our aim is to understand how microclimates caused by topographic complexity may feed back into spatial variations in tree physiology and ultimately variations in tree vulnerability to fire or mortality under stressful conditions. To do this, we embarked on a study at the University of California's Angelo Coast Range Reserve in Northern California, a site which is now NSF's Eel River Critical Zone Observatory. The focus is the temporal and cross-slope variations of sap velocities of a population of a single evergreen tree species, *Arbutus menziesii*, straddling a microclimate gradient during the dry summer.

Our study is inspired by a long history of ecological studies of plants across resource gradients (e.g., Schimper (1903); Holland and Steyn (1975); Chapin et al. (1987)), including several at fine scales which consider slope and aspect in particular (Metzen et al., 2019; Kumagai et al., 2007; Hassler et al., 2018; Renner et al., 2016; Armesto & Martinez, 1978). The cross-slope microclimate gradient underlying our study is a 'controlled laboratory' to investigate the response of sap velocities to altered temperature (T), vapor pressure deficit (VPD), and geometrically-varied light (I) regimes in particular, as other relevant environmental factors, such as precipitation, cloud cover, underlying lithology, and soil type, are comparable between adjacent hillslopes. Investigation of water dynamics in this setting provides insight into how vegetation–atmosphere water cycle interactions may evolve under future climates with different temperature and VPD regimes, which contributes to more accurate projections of anticipated water fluxes and ultimately ecosystem vulnerability under an altered climate.

The hypotheses guiding our study are that 1) slope aspect in the midlatitudes influences microclimate and hence transpiration, leading to cross-slope differences in both the timing and amount of vegetation water fluxes, and 2) occupying disparate microclimates leads to different water use habits even in a single species of tree. We present both a set of field observations and a series of modeling exercises designed to investigate the effect of disparate microclimates on water fluxes from a single species of deeply rooted, drought-tolerant, broadleaf evergreen tree. The climatic gradient created by differences in solar radiation on adjacent north- and south-facing slopes of a hill is used to explore the impact of variable microclimate on sap velocities, and thus transpiration, in this species of tree. We define microclimate by ambient air temperature and humidity beneath the canopy, incoming solar radiation adjusted for the slope and aspect of the closed canopy, and soil moisture measured at 30 cm.

In the following sections, we describe the research site and our *in situ* observations, including our hybrid observation/model approach to simulating sunlight. We then give a detailed analysis of the climatic features and sap velocity measurements of the two slopes, and present our parameterization (with a Markov Chain Monte Carlo process) of a transpiration model based on the cross-slope differences in microclimate and sap velocity. We conclude by exploring the implications of cross-slope differences in ecological response parameters for forest resilience in this region under future climates, including a discussion of the limitations of our analysis and proposed next steps.

2 Methods

2.1 Site description

Our study took place at the University of California's Angelo Coast Range Reserve (39.729N, -123.644W), a site with large variation in year-to-year precipitation (e.g., 1027 mm in 2013-14, 2991 mm in 2016-17), and hosting a heavily instrumented, steep, forested north-facing slope. The forest is composed of mixed broadleaf and needleleaf evergreen trees typical of the Pacific Douglas fir alliance (USDA, 2008).

Our installations took the observations to the opposing south slope. Because of the near-direct north–south orientation of the hillslopes, the microclimatic differences between the two slopes are pronounced. Our observations show that the south slope can be nearly 7°C hotter and experience VPDs up to 1.8 kPa greater during late Septem-

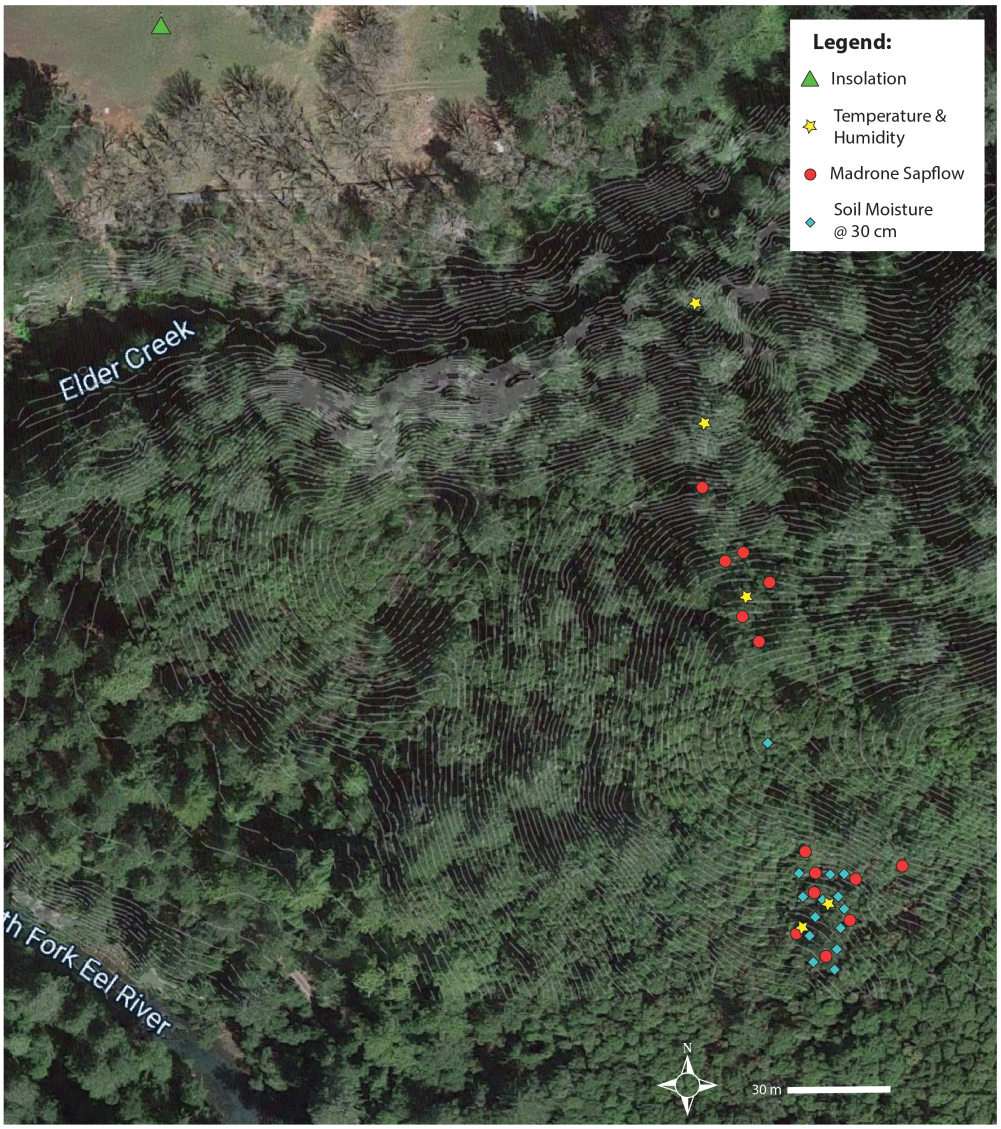

Figure 1. A map of the study site in Northern California (39.729°N, 123.644°W), and the locations of data for this analysis. The canopy covering the north slope is largely made up of Douglas fir (*Pseudotsuga menziesii*), bay (*Umbellularia californica*), and evergreen oak tree species (Tan oak *Notholithocarpus densiflorus*, Coastal live oak *Quercus agrifolia*, Canyon live oak *Quercus chrysolepis*), with some Pacific madrone trees (*Arbutus menziesii*) in the upper half of the hillslope. In contrast, the south slope is mostly populated with Pacific madrone trees, with a few Douglas fir and oak trees primarily occurring in the upper half of the slope near the ridge. One-meter topographic lines are shown in light gray. Underlying high-resolution satellite imagery is from Maxar Technologies, accessed through Google Earth Engine (Gorelick et al., 2017).

ber mornings (see Table S1). There is a visible transition in tree species composition across the ridge of the hill (see Figure 1). Because the instruments deployed across the two sides of the hill and adjacent meadow are less than 400 m apart, we assumed precipitation inputs and cloud-induced variations in solar radiation are identical for the meadow and both sides of the hill. Soil samples taken near the surface and rock cores extracted from deeply drilled wells confirmed that soil type and underlying lithology are comparable on both sides of the hill. We focus on Pacific madrone trees (*Arbutus menziesii*) because their prevalence on both slopes at our site allows for the highest possible rate of same-species sampling.

2.2 Instrumentation

The field program collected 1) sap velocity measurements on Pacific madrone trees; 2) ambient understory temperature and humidity microclimate; 3) incoming solar radiation to an open meadow adjacent to the site; and 4) soil moisture at 30 cm (Figure 1).

Sap velocity sensors (Dynamax Granier-style Thermal Dissipation Probes, as in Granier (1985) and Granier (1987)) were installed into 14 madrone trees, 8 on the south slope and 6 on the north slope (Figure 1, red dots). Our study trees ranged from 36 to 72 cm in diameter, and each tree hosted two 80-mm-long sensors (each with thermocouple junctions at 15 and 70 mm) placed approximately 180˚apart. In this analysis, we considered only data from the outer thermocouple junctions, at 15 mm depth. This resulted in 16 and 12 data streams on the south and north slopes, respectively.

Sixteen soil moisture sensors (Campbell Scientific CS650) monitored surface soil moisture at 30 cm in a network that covered the south slope and ridge area (Figure 1, blue diamonds). Unfortunately, similar soil moisture observations on the north slope were compromised during the study period, and were therefore not used in this study. Instead, we conducted a sensitivity analysis to investigate the impacts of a range of plausible moisture states on north-slope sap velocities in our modeling work. Three temperature and humidity sensors (Campbell Scientific CS215) were installed 1.5 m above the ground in weather stations on the north slope, while eleven existed on the south slope, ten of which hung in a vertical string from the canopy to the ground, and the last of which was installed 1.5 m above the ground in a weather station (Figure 1, yellow stars; vertical string

represented as one point). A weather station in an adjoining meadow provided information about incoming radiation, wind speeds, and precipitation (Figure 1, green triangle).

2.3 Data processing

All data were collected at 1–15-minute intervals and resampled to 5 minute intervals with no interpolation. Cleaning and analysis of field data was conducted with Python 3.7.4. All data and scripts for processing are available for download (Bilir, 2020).

Sap velocity: We processed our sap flow data by first applying a standard zeroing procedure to each data stream (Ward et al., 2017) using a 5-day window. After excluding outliers (one data stream on the north slope), all remaining data streams were averaged together by slope, resulting in a sap velocity time series for an average north-slope madrone tree and an average south-slope madrone tree. We interpret the standard deviation of our average-tree data streams as representing total uncertainty in our measured sap velocity magnitude. This is illustrated in Figure 2.

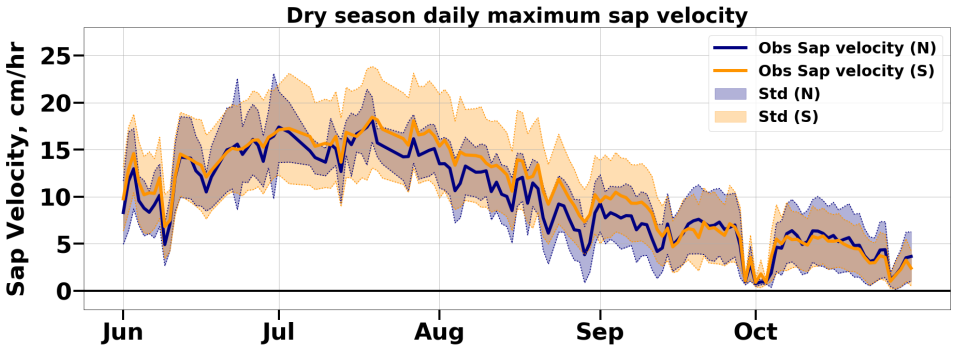

Figure 2. Daily maximum sap velocities averaged (μ) for each slope, plotted with +/-1 standard deviation (σ) reflecting spread among the data streams for each slope's tree population. The coefficient of variation ($CV = \frac{\sigma_t}{\mu_t}$, where t=time) for sap velocities on the north slope ranges from 9.5% in mid-July, to 91.0% in mid-October. The larger south slope population exhibited slightly wider spread in sap velocities on average; CV for the south slope ranges from 25.9% in mid-September to 86.0% in mid-October. The south slope has faster peak velocities on average throughout most of the dry season up to the middle of September, yet during the end of the dry season the north slope experiences faster peak sap velocities on average. Nevertheless, as Figure 5 shows, the south slope transpires more water per sapwood area even during the month of October due to a longer diurnal cycle of transpiration.

VPD: Temperature and humidity were both reported by a single type of instrument (Campbell Scientific CS215, Figure 1, yellow stars). We averaged temperature and humidity data streams by slope and then derived vapor pressure deficit (VPD) as:

$$\mathrm{VPD} = \mathrm{SVP}(1 - \mathrm{RH}) \tag{1}$$

where SVP is the saturated vapor pressure (kPa) estimated as a function of temperature by the Clausius–Clapeyron equation (Bolton, 1980), and RH is the relative humidity.

Insolation: Unobstructed total (combined direct and diffuse) solar radiation is measured in an adjacent meadow (LI-COR LI200X-L, Figure 1, green triangle). Scaling sunlight for each slope's environment from the meadow sensor is a key underlying feature of our analysis. To do this, we scaled measured total solar radiation by a theoretically-derived factor representing the relative proportion of direct-beam radiation received by each slope, based on their unique geometry. This approach is an approximation, as it does not account for the fact that the diffuse fraction of total radiation incident upon the slopes depends not on geometry, but rather on the sky view angle (i.e. horizons generated by neighboring hills) of each slope. The diffuse fraction is high under cloudy skies and at low sun angles. During our study period, clouds and fog were rare, and sap velocities were low at dawn and dusk, so the omission of partitioning and separately scaling diffuse radiation for each slope should not impact the bulk of our analysis.

To derive the sunlight scaling factor for each slope, we used: 1) slope aspect, derived from topographic maps, based on the average aspect of each sampled tree's location (the south slope's aspect is 189.1°, where 180° is due south, and the north slope's aspect is 344.2°, where 360° is due north); and 2) the canopy slope, derived from 12 LiDAR cross-sections of the vegetation (e.g. Lee et al. (2016)) on each slope (the south slope's canopy has a slope of 21.97°, while the north slope is steeper, with a canopy slope of 32.82°). We then computed idealized clear-sky direct-beam solar radiation for different times and days (solar zenith and azimuth angles) using Python's 'solarradiation' library (Stafford, 2018), which follows the formulation of Duffie and Beckman (1991). See Appendix A for details of the calculation. The calculation was done for a flat surface (S_{flat}) as well as for north and south slopes (S_{N} and S_{S}, respectively), using the latitude, canopy slope steepness, and slope aspect estimated for each slope. Then, to obtain the approximate total insolation for each slope, we scaled the total radiation measured at the meadow

by the scaling factor for each slope:

$$I_{\mathrm{N}} = I_{\mathrm{meadow,\,observed}} \times \frac{S_{\mathrm{N}}}{S_{\mathrm{flat}}} \tag{2}$$

$$I_{\mathrm{S}} = I_{\mathrm{meadow,\,observed}} \times \frac{S_{\mathrm{S}}}{S_{\mathrm{flat}}} \tag{3}$$

Figure 3 provides a visualization of the computed solar trajectories for our study site and the scaling factors based on direct-beam radiation for each slope. The relative angles of the hillslopes and solar trajectories illustrate why it is that early in the dry season, the north slope receives more afternoon sunlight than the south slope, and late in the dry season, the north slope gets very little direct sunlight at all. Late in the dry season, the south slope receives more sunlight than the flat meadow, while the north slope receives less.

Soil Moisture: Our dense network of 14 soil moisture sensors at 30 cm (CS650 Water Content Reflectometers, Figure 1, blue diamonds) shows large-magnitude variation in soil volumetric water content at a roughly 15 m length scale, independently confirmed by manual soil sampling. Analyses of soil texture and soil water retention conducted by another team working at this site show that there are no significant differences between the two slopes in these variables, rendering the relationship between soil volumetric water content and water freely available to tree roots comparable in the shallow soil layers of both slopes (Rempe, 2021). This variation in shallow soil moisture is spatially organized, and appears to relate to the geomorphology and history of shallow landslide disturbance in the area. The variation is not correlated with variation in sap velocity magnitude of proximate trees, suggesting lateral and vertical extents of the tree roots may be accessing moisture from a wider area and from deep moisture in weathered bedrock, in line with previous findings at this site (Rempe & Dietrich, 2018; Vrettas & Fung, 2017). Unable to observe these deep moisture reservoirs, we used observations of water table dynamics from 16 wells on both slopes to understand that, once the rains cease, the overall dynamics of root-zone moisture are closely correlated with those of 30-cm soil moisture over the summer dry season (i.e., both show a steady decline). We thus used an area-averaged 30-cm soil moisture to stand in for deep root zone moisture on the south slope in our model analysis. For the north slope, even lacking surface observations we knew that soil moisture would also show a steady decline throughout the dry season, though its rate of decline was not available. We therefore conducted, in the sap velocity model described below, a sensitivity analysis that considered five scenarios

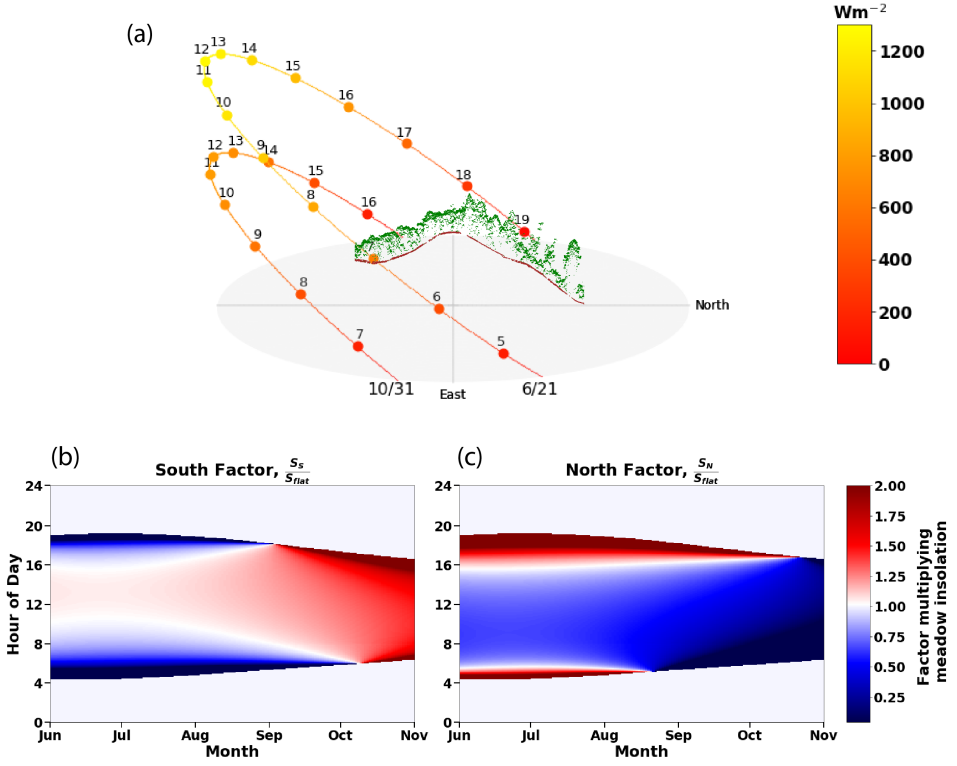

Figure 3. A summary of the solar model. Panel a: The solar trajectories at the latitude of the study site for the summer solstice (6/21) and the end of the dry season (10/31), showing that the sun rises and sets north of due East and due West for part of the dry season. The numbers indicate local time. A LiDAR cross section of the Rivendell site is provided for orientation. Panels b) and c): the scaling factor derived for each slope's direct-beam insolation relative to the meadow's direct-beam insolation, as it evolves throughout the day (y-axis) and the dry season (x-axis). The asymmetry in panels b) and c) reflects the slightly westward aspect of both slopes, also visible in Figure 1.

for north-slope soil moisture over the dry season, one of which was identical to the south-slope moisture state. The four alternative north-slope moisture scenarios varied from the south-slope soil moisture data stream in ways informed by manual soil sampling and our sap velocity observations, and included simple offsets as well as varied rates of moisture decline over the dry season. See section 3.2.1.

2.4 Modeling

For the purpose of examining cross-slope differences in sap velocity, our analysis is focused on the dry months (June–October). This time frame highlights the relationships between sap velocity and environmental conditions in four ways: 1) we eliminated conditions of post-rain leaf wetness, which could result in sunny conditions with low transpiration; 2) soil moisture at 30cm and at depth decreases monotonically; 3) we largely eliminated cloudy-sky conditions so that solar radiation can be estimated from geometric considerations; and lastly, 4) during a time of continuously declining subsurface moisture availability, we hypothesize that above-ground microclimatic variations may have the largest impact.

2.4.1 Description of sap velocity model

To quantify the relationship between sap velocity dynamics and environmental drivers for each slope, we derived a model of sap velocity tailored to the measurements available. Our derivation began from the work of Link et al. (2014), who, in order to understand the seasonal dynamics of daily maximum sap velocity across different tree species on the north slope of this site, applied the conceptual framework of the Jarvis model (Jarvis, 1976), in which the maximum bulk canopy conductance (g_{cmax}) under ideal conditions is modulated by ambient conditions to yield the instantaneous bulk canopy conductance, g_{c}. Furthermore, by assuming total transpiration E, approximated as $E = g_{\mathrm{c}} \times \mathrm{VPD}$, is proportional to the normalized sap velocity v_{n} with a proportionality constant α: $E = \alpha \times v_{\mathrm{n}}$, they obtained the equation:

$$v_{\mathrm{n}} = \frac{g_{\mathrm{cmax}}}{\alpha} \times \mathrm{VPD} \times f_{\mathrm{VPD}}(\mathrm{VPD}) \times f_{\theta}(\theta) \times f_{\mathrm{I}}(I). \tag{4}$$

The forms of the functions are taken from Lohammar et al. (1980), Feddes et al. (1978), and Waring and Landsberg (2011):

$$f_{\mathrm{VPD}}(\mathrm{VPD}) = \frac{1}{1 + \frac{\mathrm{VPD}}{D_0}}, \tag{5}$$

$$f_{\theta}(\theta) = \frac{1}{1 + \exp(-\beta(\theta - \theta_0))}, \tag{6}$$

$$f_I(I) = \gamma(I - 1000) + 1, \tag{7}$$

where D_0, β, θ_0 and γ are parameters determined for each tree species using daily maxima of normalized observed sap velocity, VPD, insolation and soil moisture from February 2009 to October 2011.

Equation 4, developed to investigate the seasonality of normalized daily maximum sap velocity across tree species on the same slope (and same microclimate), is not applicable for modeling the diurnal cycle during the dry season, where hysteresis in the response of sap velocity to VPD and insolation is observed (Zhang et al., 2014; Gimenez et al., 2019). We modified Equation 4 by allowing for a lag in the sap velocity response to diurnally cycling VPD and insolation of 1 and 2 hours previous, resulting in Equation 8. We chose these time frames based on observed lags in our data (see Figure 4). Because we did not see substantive diurnal variations in soil moisture θ in our data, we did not include lagged terms for Φ_θ in Equation 8. We further modified the approach by using sensor-averaged rather than normalized sap velocities, which provided the best match with the scale of our environmental data (see Section 2.3). Using sensor-averaged rather than normalized sap velocities and splitting the Φ_{VPD} and Φ_I expressions into three led to scaling differences in our parameters compared to Link et al. (2014), and in particular, our initial constant, the analog of g_{cmax}/α, has less relation to a theoretical maximum bulk canopy conductance, so for clarity we rename it ε. The resulting model for sap velocity v_{s} is:

$$
\begin{aligned}
v_{\mathrm{s}}(t) &= \varepsilon \times \Phi_{\mathrm{VPD}}(\mathrm{VPD}_t, \mathrm{VPD}_{t-1}, \mathrm{VPD}_{t-2}) \times \Phi_\theta(\theta_t) \times \Phi_I(I_t, I_{t-1}, I_{t-2}) \\
\Phi_{\mathrm{VPD}} &= \frac{\mathrm{VPD}_t}{1 + \frac{\mathrm{VPD}_t}{D_0}} \times \frac{\mathrm{VPD}_{t-1}}{1 + \frac{\mathrm{VPD}_{t-1}}{D_{-1}}} \times \frac{\mathrm{VPD}_{t-2}}{1 + \frac{\mathrm{VPD}_{t-2}}{D_{-2}}} \\
\Phi_\theta &= \frac{1}{1 + \exp(-\beta(\theta - \theta_0))} \\
\Phi_I &= (\gamma_0(I_t - 1000) + 1) \times (\gamma_{-1}(I_{t-1} - 1000) + 1) \times (\gamma_{-2}(I_{t-2} - 1000) + 1),
\end{aligned}
\tag{8}
$$

where t is time and t_{-1} and t_{-2} denote 1 and 2 hours previous, respectively. This results in additional parameters in Equation 8, D_0, D_{-1}, D_{-2}, γ_0, γ_{-1}, and γ_{-2}, in addition to β and θ_0.

2.4.2 Estimation of Slope-specific Parameters

We used Hamiltonian Monte Carlo (Betancourt, 2017), a type of Markov Chain Monte Carlo, and the No-U-Turn Sampler (Hoffman & Gelman, 2014) to derive our parame-

ters in Equation 8 for each slope. Parameter estimation used the pymc3 package in Python (Salvatier et al., 2016). For each slope, we randomly selected 20% of the data (non-sequentially) and assigned it to a training data set, while reserving the remainder for testing model performance. We repeated this procedure five times, to ensure that parameter estimates did not change substantively depending on the sample assigned to the training data set. Our final reported parameters are the mean of the parameters arising from each of the five parameterizations for each slope. Details on how we selected priors and how the posteriors compared to priors are given in the supplement accompanying this paper.

2.4.3 Assessment of model performance

To assess model performance, we used root mean squared error (RMSE), a scale-dependent measure, as well as normalized root mean squared error (nRMSE), a scale-independent measure:

$$\mathrm{RMSE} = \Big(\sum_{n=1}^{N_{\mathrm{obs}}} \frac{(\widehat{v_{\mathrm{s},n}} - v_{\mathrm{obs},n})^2}{N_{\mathrm{obs}}}\Big)^{1/2}, \tag{9}$$

$$\mathrm{nRMSE} = \frac{\mathrm{RMSE}}{\big(v_{\mathrm{obs,\,max}} - v_{\mathrm{obs,\,min}}\big)}; \tag{10}$$

$\widehat{v_{\mathrm{s},n}}$ and $v_{\mathrm{obs},n}$ are the modeled and observed sap velocities, respectively. This is reported in section 3.3, as well as shown in figures 8 and 7.

We additionally examined residual errors in the context of model inputs and other contextual information. This is discussed in section 3.3.1.

2.4.4 Model experiments

An examination of model parameter differences is not, in isolation, an intuitive way to understand vegetation response differences. Therefore, to understand the disparate sensitivities of sap velocity to microclimate between these two populations, we carried out two sets of model experiments with our derived models of sap velocity, driven by ambient environment, for each hill slope. The first set of experiments involved supplying the same diurnal cycle of VPD and insolation for both slopes and examining each functional expression of the model separately. In the second set of experiments, we performed a series of 'climate swaps' in which the model for one slope was given the total microclimate, or VPD and insolation alone, of the other. These are described section 3.4, as well as figures 9 and 10.

3 Results & Discussion

3.1 Microclimate and sap velocities on the north and south slopes

The high-frequency data streams for June–October 2018 include the sensor-averaged microclimate and sap velocities for the north and south slopes, as well as the sensor-averaged soil moisture for the south slope. While soil moisture declines through the dry summer, sap velocities on both slopes peak in July when 30-cm soil moisture is ∼10%, about 1-2 months after the start of the dry season. The north-slope insolation declines as the summer progresses into early autumn, while insolation on the south slope remains approximately constant. VPD on both slopes fluctuates, depending on whether winds are onshore or off-shore, but shows no seasonal trend (Figure S1).

Monthly climatologies of the diurnally cycling variables (i.e., all except soil moisture) display the microclimate and sap velocity differences between the two slopes, and provide a snapshot of how these variables evolve together throughout the dry season (Figure 4). As expected from Figure 3, noontime insolation on the south slope is nearly double that of the north slope from August until October, leading to instantaneous air temperature differences of up to ∼7°C and VPD differences of up to 1.8 kPa (Table S1). In the late afternoons of early summer through mid-August, insolation is greater on the north slope than on the south slope (see Figure 3), leading to brief (∼2-hour) periods of higher air temperature, VPD, and sap velocity on the north slope. A symmetrical period of greater insolation in the early mornings does not materialize, due to a slight westward aspect of both slopes (see Figure 1). Both the south and north slopes show sap velocities that peak, not surprisingly, around mid day. However, the south-slope sap velocity is substantially faster than north-slope sap velocity in late morning, while the north slope flows slightly faster than the south slope in the late afternoon and early evening in the early summer. The cross-slope dynamics of the sap velocity diurnal cycles thus reflect the cross-slope dynamics of the diurnal cycles in above-ground microclimate.

Figure 5 underscores the differences between the two slopes in timing and amount of sap velocity in the diurnal cycle. We use time-integrated sap velocity as a proxy for transpiration on each slope, assuming that tree populations have equivalent sapwood area in trunks of equivalent diameter. Under this assumption, on average, south-slope madrones transpire 20% more water per day over their combined sapwood area during the dry season. August shows the largest percentage differences in transpiration, with south-slope

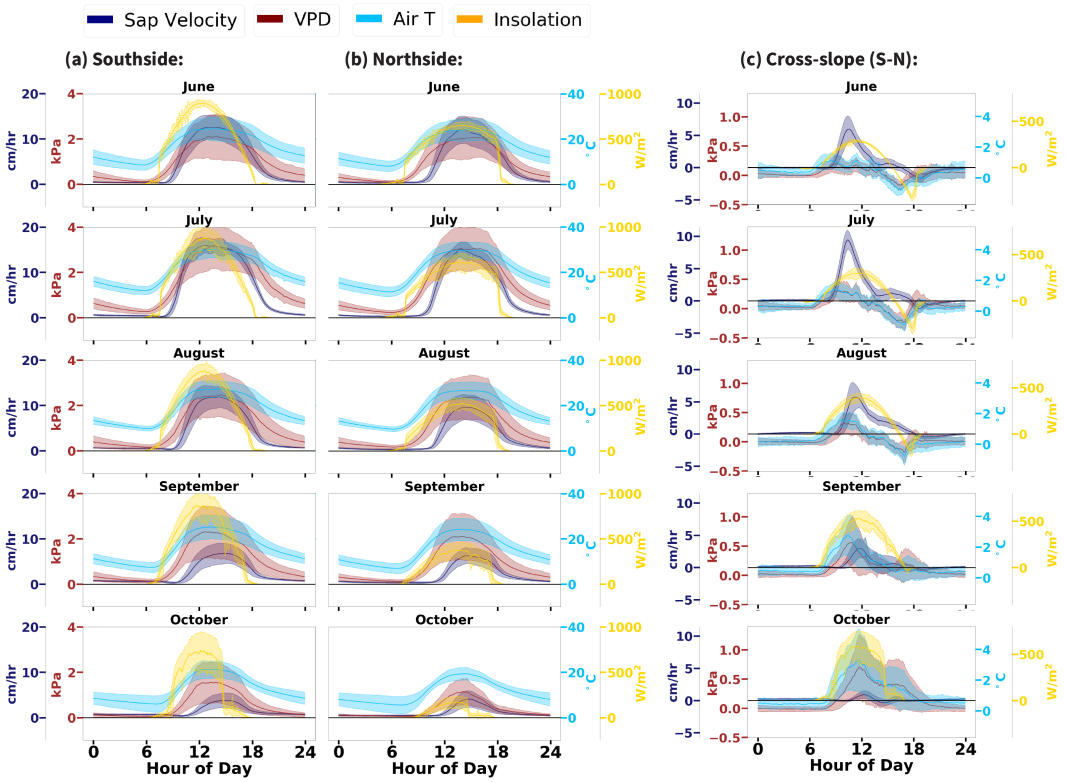

Figure 4. Monthly climatologies of diurnally cycling environmental drivers of sap velocity for the south slope (panels of column (a)), the north slope (panels of column (b)), and for the cross-slope differences (panels of column (c)). Shading shows +/- 1 standard deviation of the monthly climatology, and thus reflects the variability over the month. For all the months of the dry season and on both slopes, air temperature (pale blue) rises and falls in close concert with the sun (yellow), while the VPD diurnal cycle (burgundy) lags behind, and sap velocity (purple) lags behind even further. Though cross slope differences in sap velocity peak in July, the cross-slope microclimate differences peak in the late dry season, in September and October.

madrones transpiring on average 32% more water per day over their combined sapwood area during this month. While for most of the dry season the average south-slope madrone tree moves water as fast or faster than the average north-slope madrone tree at their respective moments of daily peak sap velocity, Figure 2 shows that late in the dry season the north slope madrone trees are slightly faster, although they still transpire less per day.

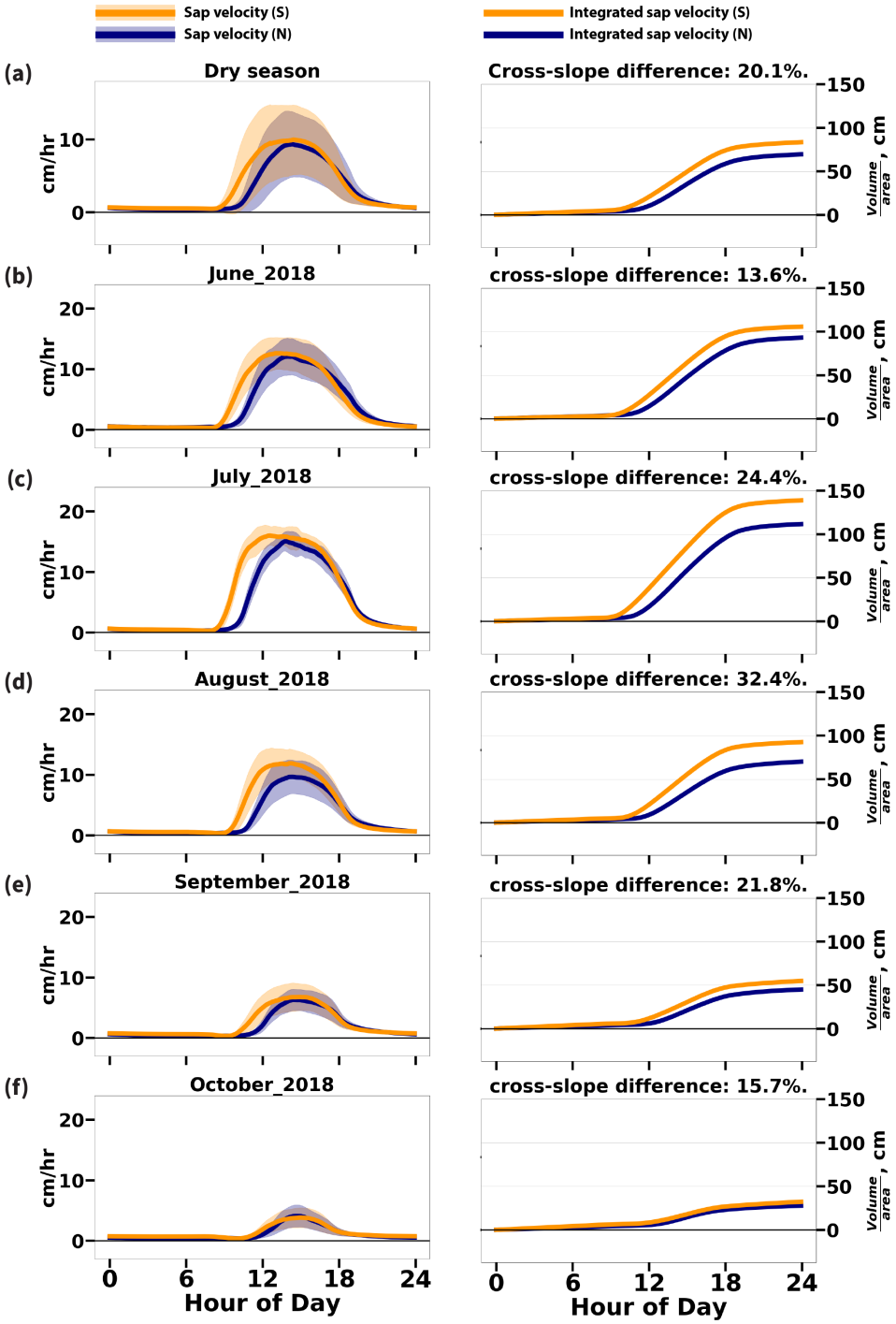

Figure 5. See next page for caption.

3.2 Model Parameters

The probability density distributions of the Equation 8 parameters estimated for the north and south slopes are shown in Figure 6. The means and standard deviations of the priors and posteriors of the parameters are shown in Table S2.

Figure 5. (on previous page) Average diurnal cycles (left panels) and cumulative integrals (right panels) of sap velocity for the entire dry season (panels in row a) and by month (panels in rows b-f). Time-integrated sap velocity, used here as a proxy for transpiration, results units of centimeters, which can be understood as volume per area (right-hand axis), or put another way, the average distance water travels up the trunks, through the trees' combined sapwood area. The north slope is shown in purple and south slope is shown in orange; shading shows +/- 1 standard deviation of the climatologies, reflecting the variability over the time period (month or dry season). The south slope exhibits higher rates of time-integrated sap velocity, a proxy for transpiration, beginning earlier in the day and also experiencing a longer stretch of high sap velocity. Later in the day, the north slope experiences faster peak sap velocities, although it still produces less cumulative transpiration. See Figure 2.

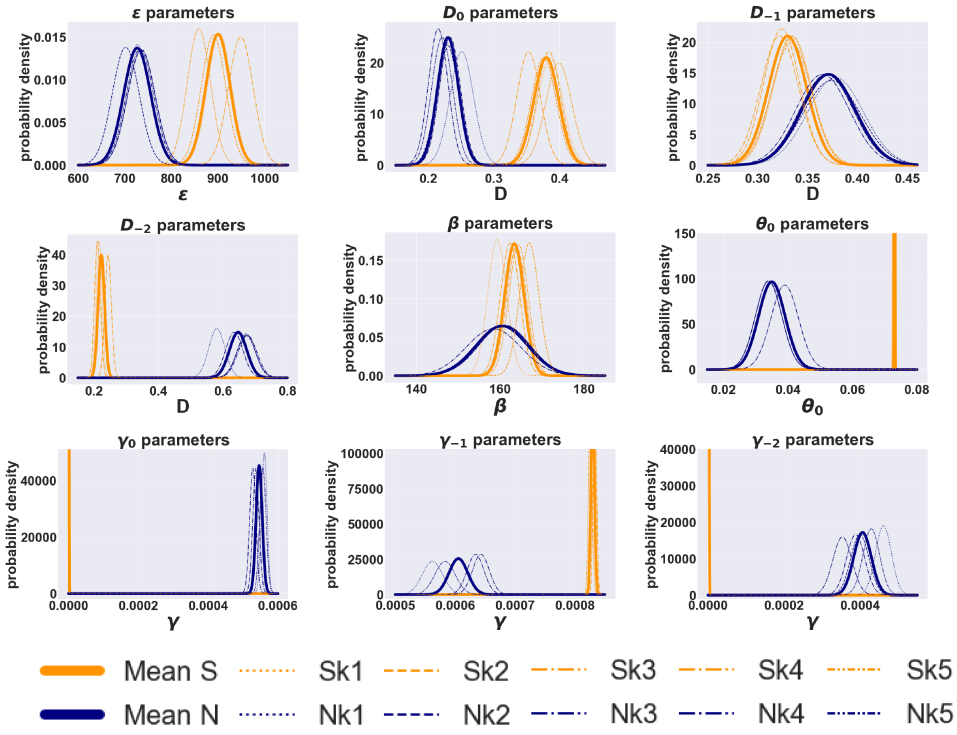

Figure 6. Posterior distributions of fitted model parameters for the north slope (blue) and south slope (orange). Results from each of the five randomly-selected training datasets are shown as dotted lines, and the mean as a bold line. Different subsets of data (k1-k5) used to parameterize the model result in very little difference in the fitted parameters, which is demonstrated in the narrow spread among the thin dotted lines.

The resulting parameters for each slope show key differences in response to environmental drivers. With the VPD parameters D_0, D_{-1} and D_{-2}, a larger parameter value points to a greater sap velocity sensitivity to the variable (see Equation 8). The south slope has D_0, D_{-1} and D_{-2} values of 0.38, 0.33, 0.22, respectively, suggesting that south-slope sap velocities are most sensitive to instantaneous VPD, but also to VPD from 2 hours prior, though lagged VPD plays a slightly smaller role. The corresponding values for the north slope are 0.22, 0.34 and 0.80, suggesting that on the north slope VPD_{t-2} has the largest influence on sap velocities.

For insolation, the γ_0 and γ_{-2} for the south slope are near zero, suggesting that sap velocities there respond mainly to insolation of the past hour (I_{t-1}). For the north slope, the results suggest that sap velocities are sensitive to contemporaneous insolation as well as insolation of the past two hours, as γ_0, γ_{-1} and γ_{-2} have comparable values.

For soil moisture, β controls the slope of the sigmoid, and θ_0 controls the midpoint. When soil moisture data input is identical for both slopes, β is similar between the two slopes, while θ_0 for the north slope is lower than that of the south slope by a factor of two. The partial function Φ_θ (see Figure S2, panel d) shows that while soil moisture is a strongly limiting factor on south-slope sap velocities below $\sim$10%, it causes no such limitation for north-slope sap velocities. Because soil moisture creates no constraint on sap velocities in the north-slope model, there is less certainty in the exact parameter values, as seen in the larger spread of the north-slope parameters β and θ_0 compared to the south slope (Figure 6).

3.2.1 Parameter sensitivity to north-slope soil moisture scenarios

As mentioned in Section 2.3, we lack surface soil moisture observations on the north slope. This missing data leaves the true values of β and θ_0 uncertain on the north slope. Because of the multiplicative model formulation, differences in these parameters and the value of the Φ_θ function could, in turn, impact the values of the other expressions and parameters in Equation 8, rendering the entire north-slope sap velocity response to microclimate uncertain. Our field experience and our sap velocity data streams show that north-slope soils are as wet or wetter than those of the south slope, presumably due to unequal evapotranspiration demand. Therefore, the north-slope soil moisture scenarios we explored in our sensitivity experiments began with the south-slope data stream and

increased the soil moisture in both uniform and non-uniform ways. The scenarios were as follows: 1) we added a uniform 5% increase to observed south-slope soil moisture; 2) we adjusted the rate of soil moisture decline to half of the rate observed on the south slope, which amounted to a +5% difference in soil moisture by the end of the dry season; 3) we adjusted the rate of soil moisture decline to one third of the rate observed on the south slope, which amounted to a +7% difference in soil moisture by the end of the dry season; and lastly, 4) we added a uniform 2% increase to observed soil moisture, and then additionally adjusted the rate of soil moisture decline to half of the observed rate, which amounted to a +7% difference in soil moisture by the end of the dry season. We then reran the north-slope MCMC parameterization process with these alternative soil moisture states, and compared them with a standard run in which we matched soil moisture for both slopes to the area-averaged south-slope moisture state.

We found that between the standard and sensitivity experiment parameterizations, none of the final parameters changed substantively except θ_0 (Table S2). The changes in θ_0 that resulted do not change the shape of Φ_θ, but rather shift it along the θ-axis, tracking the new (higher) seasonal minimum implied by the alternative moisture scenarios (see Figure S2). The function Φ_θ did not decline below a value of 1 throughout the seasonal range of moisture hypothesized in each scenario. Thus, we conclude that, in our model formulation, the relations among the north-slope data streams indicate no sap velocity constraint by soil moisture, and that this conclusion is not sensitive to a plausible range of soil moisture states for the north slope.

3.3 Model performance

With slope-specific parameters in combination with slope-specific microclimate data streams, we computed model sap velocities for north and south slopes. From our final parameter distributions for each slope, we sampled 10,000 subsets of parameters, which, combined with the environmental data streams, generated an ensemble of modeled sap velocity time series consistent with the uncertainty in the model parameters for each slope. These ensembles were then used to generate the modeled sap velocity climatologies and modeled daily integrals reported in Figures 7 and 8.

The modeled sap velocities compare well with those observed. The model captures 88% and 89% of the June–September daily integrated sap velocity on the north and south

385 slopes, respectively. The performance of the daily integrals deteriorates to 77% for both slopes when October is included. The reasons for this are addressed in Section 3.3.1.

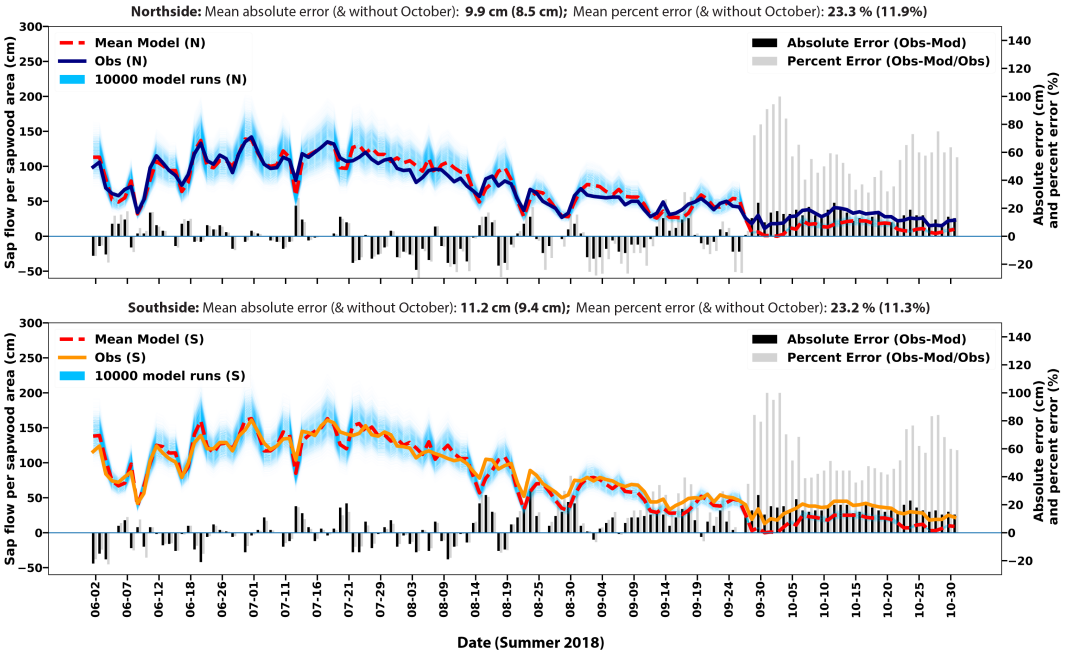

Figure 7. Daily integrated sap velocity yields a daily distance that water moves up the tree trunks over the combined sapwood area of the study population for each slope, which serves as a proxy for daily transpiration. Here we plot modeled (light blue lines with red dashed line representing the mean model run) and observed (orange line for the south and dark purple line for the north) daily integrated sap velocity for each slope, with the bars underneath representing both the absolute error in the model (black bars, units of cm) and the percentage error (light grey bars, unitless). The spread among the model runs is a visual indication of model uncertainty arising from spread in the parameter estimates. Error is computed relative to the magnitude of the observations, with positive errors indicating a model underestimate and negative errors indicating a model overestimate. The month of October is underestimated due to seasonal shading of the light sensor positioned in the meadow, which is not representative of the tree environment at low sun angles. For the north slope, the model is able to capture 77% of dry season integrated sap velocity, and 88% of June–September integrated sap velocity. For the south slope, the performance is similar, with 77% of dry season integrated sap velocity and 89% of June–September integrated sap velocity represented.

386

A comparison of the mean diurnal cycle of the sap velocities and their dry season integrals is shown in Figure 8. The nRMSE is 4% and 5% for the north and south slopes, respectively, and increases to 5% and 6% when data for only 7am to 10pm are included (i.e., the dynamic portion of the day). The models capture 75% of the cross-slope difference in seasonal integrated sap velocities.

In summary, Equation 8 with the slope-specific parameters captures the main features of the observations.

3.3.1 Examination of residuals & limitations of analysis

The month of October stands out as a period of systematic error in Figure 7. There are several reasons. Firstly, the representation in a rough terrain of sunlight on the slopes scaled from a flat meadow observation becomes less accurate as the solar arc becomes lower in the sky (i.e., closer to the winter solstice). This is because the diffuse fraction of radiation becomes significant at low sun angles, when shading from neighboring hills, especially in early morning and late afternoon, plays an important role. In particular, the hill-shading received by our meadow-based light sensor begins substantially earlier in the day, in the late dry season, than the shading experienced by the trees under observation, which are positioned at a higher altitude. These factors account for the model predictions of sap velocity being artificially low compared to observations, as they are based on 1) a solar day in the low meadow that is 1-2 hours shorter than the trees on the slopes experience, and 2) insolation scaling appropriate for direct-beam insolation only, even though the fraction of diffuse radiation is potentially high or unequal between the slopes due to shading from neighboring hills on late October afternoons. Secondly, we note that October began with a rain storm which was the only substantive moisture input during the period under observation. This rain event likely altered the relationship between surface and deep moisture reserves compared to the rest of the dry season, confounding the relationship between our 30-cm soil moisture data and the deeper root zone moisture available in the month of October.

Apart from the month of October, the errors seem randomly distributed. We looked for, but did not find, correlations with wind speeds both in the time series and integrated over days. However, we can identify loose correlations of the residuals with daily inte-

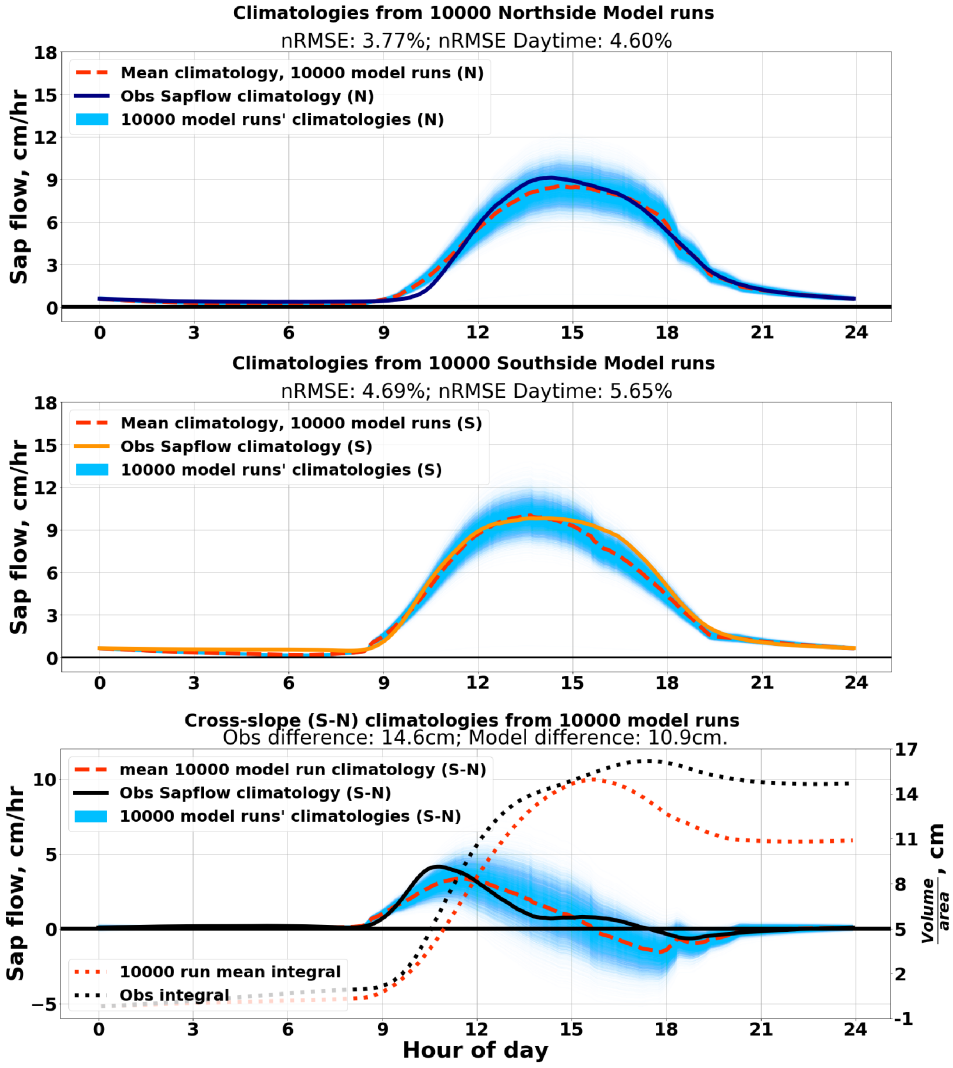

Figure 8. Performance assessment of models relative to the dry season average diurnal cycle. Dry season climatologies of 10,000 model runs are in pale blue, with the mean in red, and observed sap velocity in orange for the south and dark purple for the north. The spread among the 10,000 model runs is a visual indication of model uncertainty arising from spread in the parameter estimates. The normalized root mean square error (nRMSE) of the model comparison to observations is computed relative to the mean of the model runs, and is roughly 4% and 5% for the north and south slopes respectively (top two panels); if error is computed only over the active portion of the diurnal cycle (7am-10pm), this rises to 5% and 6% nRMSE for the north and south models respectively. The models are able to capture 75% of the observed difference in time-integrated sap velocity between the slopes (bottom panel).

grated VPD. This suggests that there is a slight bias in our model towards overestimating sap velocity on exceptionally dry days, and underestimating it on more humid days.

3.4 Sensitivities of Sap Velocities to Microclimate

At the heart of our analysis is the question of whether cross-slope differences in sap velocity are proportional to the cross-slope differences in microclimate, or whether population-level differences in physiological function also play a role. Though the individual parameter differences in our sap velocity model suggest population-level differences in water usage sensitivity to environmental drivers, we sought a more intuitive way to understand these parameter differences in aggregate. We used two sets of model experiments to show the difference in vegetation response to environmental drivers between the two slopes.

3.4.1 Model Experiment 1: same microclimate

In the first set of experiments, we computed mean diurnal cycles of VPD and insolation for the south environment in July, and used these mean cycles as inputs to Φ_{VPD} and Φ_I for both slopes (see Equation 8). Figure 9 shows the hysteresis loops in the sap velocity responses. For the same VPD diurnal cycle, the north-slope model's Φ_{VPD} attributes more sap velocity amplitude variations to variations in VPD than does the south-slope model. Also, at every value of VPD, the north-slope model has a larger sap velocity response than the south-slope model. This shows that the north-slope model has both a higher baseline response to VPD as well as a higher proportional response to increases in VPD than the south-slope model.

The south slope Φ_I has higher values than the north slope over the range of observed sunlight, and covers a slightly larger range on the y-axis. This implies that modeled sap velocity on the south slope has a higher baseline response to sunlight, and a slightly more sensitive response to increases in sunlight.

Lastly, the south slope's soil moisture function shows soil moisture to be a limiting factor on sap velocities, while conversely the north slope shows no moisture constraint, within the range of observed soil moisture over the whole season.

Taken together, the model results indicate population-level differences in response to environmental drivers of transpiration. This is explored further in Section 3.5.

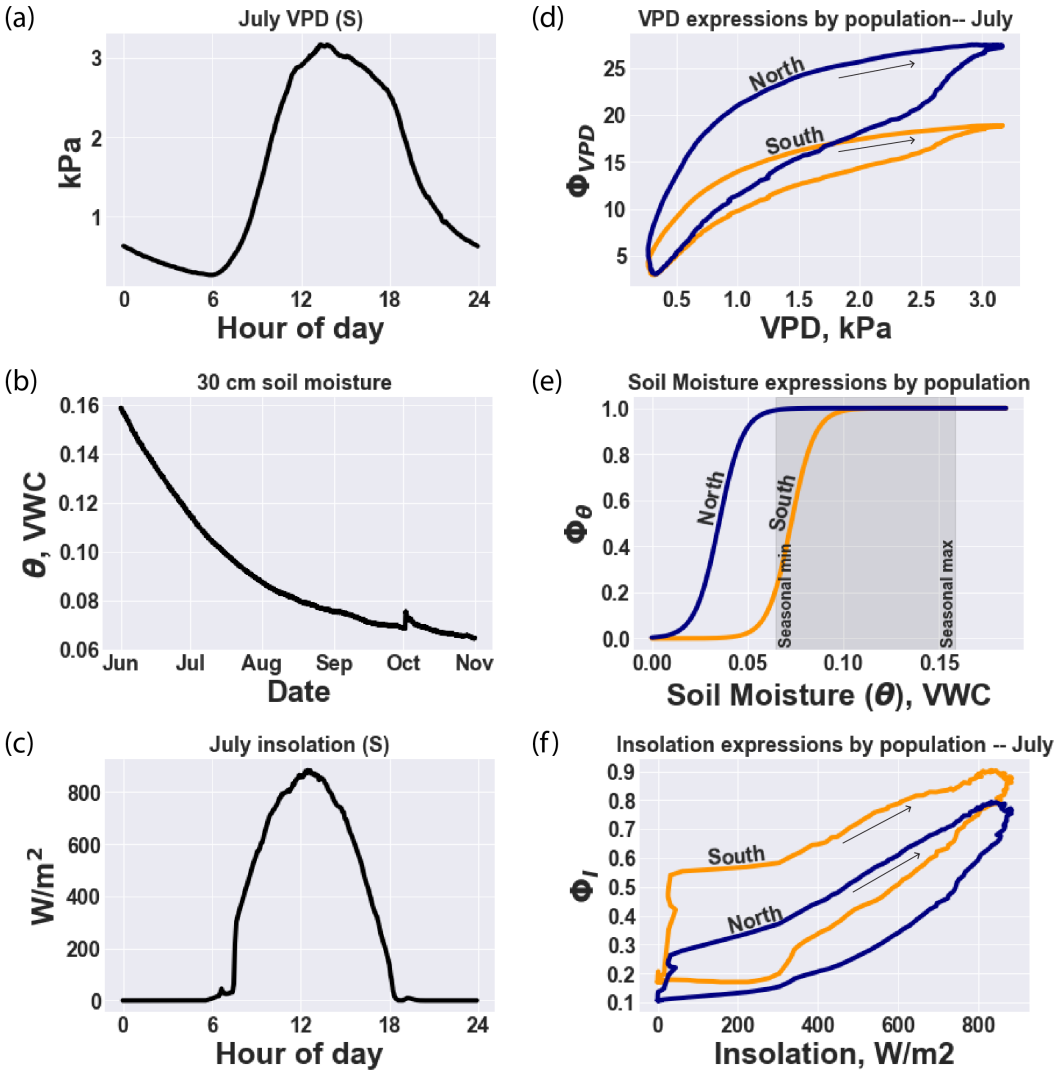

Figure 9. Partial expression plots of Equation 8 show differing sensitivity to environmental drivers among the two populations (right side panels), when fed identical data streams (left side panels). The north slope model is more sensitive to VPD, and less sensitive to soil moisture and insolation, indicating that the trees on the north slope do not feel additional transpiration constraint from drying soils over the course of the dry season, beyond that imposed by the light limitation.

3.4.2 Model Experiment 2: Influence of parameters vs microclimate

In the second series of experiments, we exchanged some or all of the experienced microclimate between the models for each slope, as a way to observe the differences in environmental responses between the two models. This experiment is visually summarized in Figure 10.

The north-slope model substantially overestimates sap velocity in the south-slope microclimate, and the south-slope model underestimates sap velocity in the north-slope microclimate. Further, exchanging VPD environment while maintaining the native light environment makes very little difference; in contrast, exchanging the solar radiation environment while maintaining the native VPD environment makes a large difference to modeled sap velocities. Lastly, artificially increasing soil moisture increases the sap velocities on the south slope, but not the north slope.

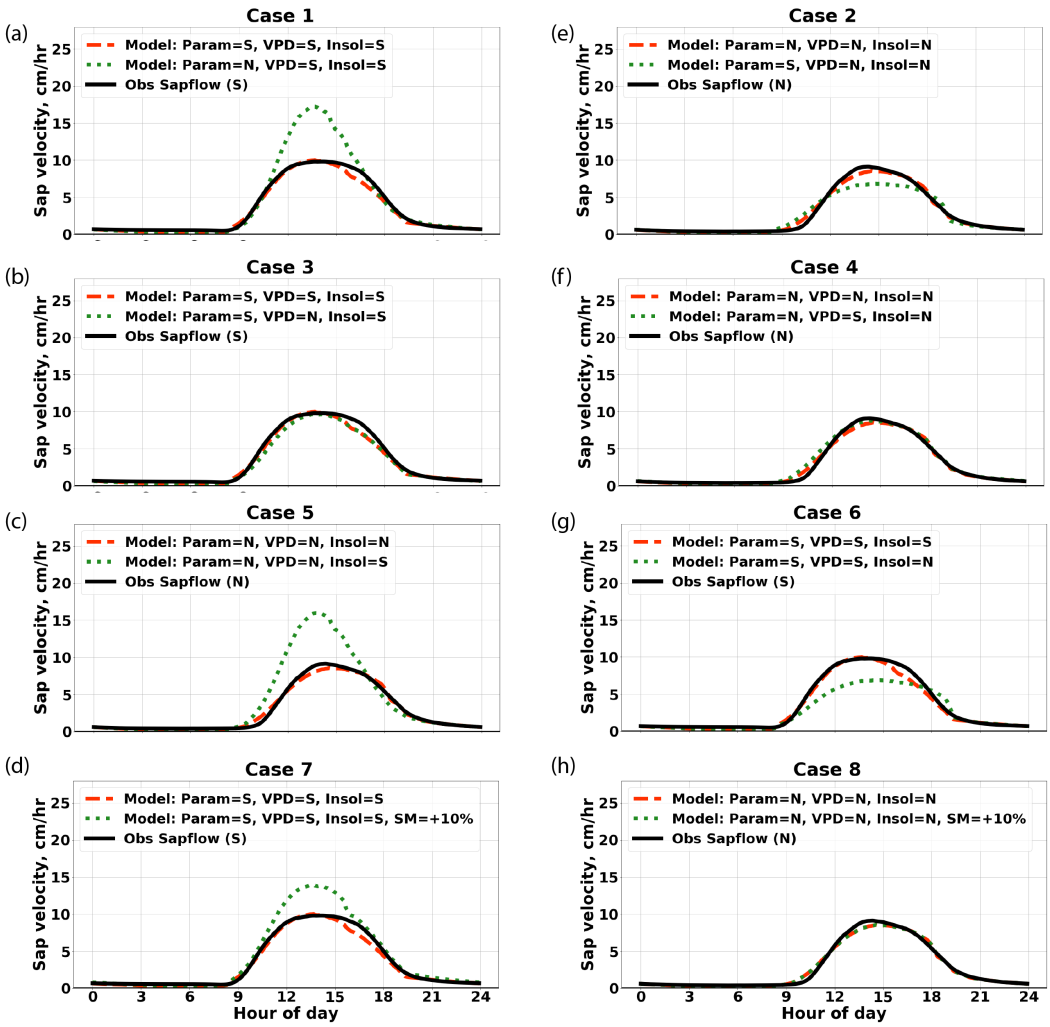

Figure 10. (See next page for caption.)

The individual responses to environmental drivers, Φ_{VPD}, Φ_θ, and Φ_I (Figure 9) show that the overestimation of sap velocities by the north-slope model in the south-slope microclimate is not associated with a stronger response to light from north-slope trees,

Figure 10. (Figure on previous page) Using the slope-specific models in the opposite slope's microclimate shows the differences in response generated by the two parameterizations to the same microclimate. Case 1 shows that the north model in a south microclimate (dotted green line) has a more vigorous response than both the south model (dashed red line) and the observations (solid black line) in the same microclimate, while conversely Case 2 shows that the south model in a north microclimate (dotted green line) underestimates both the north model (dashed red line) and observations (solid black line) in the north microclimate. Cases 3-8 break down the sensitivity by examining the impact of exchanging only one environmental variable at a time. While exchanging only the VPD portion of the microclimate between the two slopes makes almost no difference to the sap velocities estimated by each model (compare the dashed red and dotted green lines in Cases 3 and 4), exchanging the solar radiation environment makes a large difference (compare the dashed red and dotted green lines in Cases 5 and 6). Furthermore, reiterating Figure 9 panel (e), Cases 7 and 8 show that increased soil moisture increases predicted sap velocities in the south model, but not in the north model. The estimation by the north model of faster sap velocities than the south model in the south microclimate (Case 1) is due in roughly equal measure to the north model's lack of soil moisture constraint and more vigorous response to VPD. The radiation exchange (as seen in isolation in Cases 5 and 6) appears to produce most of this result because it frees the north slope model from serious light limitation.

but instead with firstly a lack of moisture limitation on sap velocities, and secondly with a stronger response to VPD. Once the north-slope model is freed from its light-limited environment by using south-slope insolation, the added vigor of its VPD response compared to the south-slope model becomes clear.

3.5 Interpretation of sap velocity model results

The divergent parameterizations indicate different physiological responses to environment between the two slopes, after controlling for inhabited microclimate. None of the parameters in our model is a direct metric of a particular physiological property of the trees, but they do represent an aggregation of functional or "behavioral" differences, integrated across all mechanisms that influence sap velocity response to ambient environment (Jarvis, 1976; Lohammar et al., 1980). Extrapolations of disparate physiological properties between the two tree populations from the differences in the mod-

els' parameters are speculative, but we explore these speculations to begin a discussion about the degree and kind of acclimation that may exist between trees on differing slope aspects. We consider the differences in each partial function Φ in turn.

VPD: Comparison of Φ_{VPD} in each model indicates that north-slope madrones are more sensitive to shifts in VPD than their south-slope counterparts (Figure 9). This is corroborated by several lines of reasoning. Firstly, because of the stark differences in light environment between the two slopes of the hill, we expect that the relative abundances of sun-adapted and shade-adapted leaves differ in the overall composition of the madrone canopies representing each slope's population, with the north slope presumed to have more shade-adapted leaves than the south slope. There is a substantial body of literature describing the physiological differences between sun-adapted and shade-adapted leaves (Boardman, 1977; Larcher, 1995), but because these differences are usually described in terms of carbon assimilation rather than water use, relating them to differences in transpiration dynamics between the two populations is challenging. To do this we would need information about relative water use efficiencies. This ties in with the second likely difference between the populations: differing canopy architectures along the lines of what is typical of sun-rich vs. shade-rich populations likely lead to differing light exposure regimes, which in turn could impact water use efficiencies on a population level. If, for instance, the proportion of leaf area accessing direct sunlight as opposed to indirect light, or even sunflecks, is less on the north slope, the north-slope transpiration dynamics could be expected to be based on lower water use efficiencies, due to differing strategies of stomatal regulation (A. Knapp & Smith, 1987; D. Young & Smith, 1979). Woody vegetation using sunflecks as a light source have been shown to leave stomata open during moments of low light in order to assimilate the most carbon when leaves are illuminated (Stokes et al., 2010; Pearcy, 1998; A. K. Knapp & Smith, 1990). Thus, such differences in canopy architecture could result in tighter coupling between sap velocity and VPD in north-slope canopies, due to the likely prevalence of exposed stomata on leaves that do not continuously experience the top-of-canopy sunlight dynamics. While the impact of differing proportions of sun-adapted vs shade-adapted leaves is obscured by an inability to resolve the exact mechanisms involved, we do suspect that this also plays a role in shaping the differences we observe. We thus speculate that, due to both lower light levels and disrupted exposure to what light there is, north-slope trees are comparatively profligate wa-

ter users even in the midst of the dry summer, preferring to maximize carbon assimilation rather than conserve water.

Soil Moisture: Φ_θ indicates that north-slope madrones are not water limited over the dry season. In our model, artificially increasing soil moisture for the north slope (i.e., 'watering' the trees) does not lead to increased sap velocity (see Figure 10, panel h). Nor does artificially increasing the soil moisture feeding into the MCMC algorithm alter the resulting north-slope parameters in meaningful ways (Figure S2). We hypothesize that this is because there is greater plant-available moisture on the north slope. The north slope has a deep water table (20 m) and a thick layer of weathered bedrock, and it has been shown to store around 30% of subsurface moisture in the vadose zone (Rempe & Dietrich, 2018; Vrettas & Fung, 2017). While there is evidence that trees on both slopes use this deep 'rock moisture' in the vadose zone for part of the dry season (Oshun, 2016), we have less data about the subsurface structure on the south slope, and data on respective rooting depths between the two populations is inconclusive (Oshun, 2016). However, the stronger sunlight on the south slope leads to higher evaporation, and the sap velocity data shows that the south slope trees cumulatively extract more water. Even if the subsurface structures and rooting depths were similar, there would be less soil moisture availability on the south slope. Also, the north-slope madrones grow in closer proximity to Douglas firs, which are known to exhibit hydraulic redistribution (Brooks et al., 2002, 2006), further contributing to increased moisture availability in the north-slope rooting zone.

Insolation: Φ_I indicates that south slope madrones have moderately higher sensitivity to insolation, and a larger response at every level of sunlight than the north-slope function (see Figure 9, panel c). The higher sensitivity in the insolation response on the south slope could be explained by factors similar to those influencing VPD response, namely a higher fraction of leaves exposed to direct light, leading to stomatal regulation strategies that are more in phase with changes in light than those on the north slope. The upwards shift in the magnitude of the response could be explained by higher proportions of sun-adapted leaves in the south-slope trees, which, due to their enhanced stomatal area (Boardman, 1977), could have higher rates of water use at every level of light intensity. To summarize the complementary hypotheses around stomatal area embedded in our interpretations of Φ_{VPD} and Φ_I, we hypothesize that due to speculative population differences in tree architecture, stomatal area, and stomatal regulating behavior (made pos-

sible by below-ground differences in water availability), 1) the north-slope trees have a larger area of stomata exposed under conditions that combine lower light and higher VPD than their south-slope counterparts, who, being moisture limited, close their stomata under these conditions; and 2) south-slope trees have a larger area of stomata exposed under conditions that combine higher light and lower VPD, which do not occur on the north slope.

4 Conclusions

It is known that different species of vegetation exhibit a wide range of responses to ambient environment. Here, we show that even within a single species, substantial variation in environmental response can exist, which in turn may vary the functional role that species plays in biogeochemical cycles, and future vulnerability to a range of stressors. In particular, 1) There are substantive microclimate differences between slopes; 2) Population-level sap velocity differences between tree populations inhabiting the north and south slopes indicate substantive transpiration differences between slopes; 3) A sap velocity model parameterized only with ambient microclimatic conditions captures sap velocity for our site well; and 4) The parameter differences in our sap velocity model represent different responses to ambient environment, and imply functional differences in tree physiology, between the two populations. This is suggestive of acclimation to inhabited microclimate.

Our results strongly hint at acclimation in leaf and canopy structure and differing stomatal regulation strategies (as in Wang et al. (2020)) between the two populations of trees. We suggest that north-slope trees, limited by sunlight rather than soil moisture, have developed their canopies and stomatal regulation strategies to optimize for light capture while spending water more profligately than their south-slope counterparts. Through this optimization, the north slope may be presumed to have different rates of carbon fixation per area of leaf and unit water transpired. This has implications for understanding water and carbon fluxes from forests today, and also for anticipating population-level profiles of vulnerability to future conditions.

Climate change is expected to alter current regimes of temperature (increase, Romero-Lankao et al. (2014)), VPD (increase, Grossiord et al. (2020)), precipitation (slight increase, although with decreased water availability, Romero-Lankao et al. (2014); Zamuda

et al. (2013)), and cloudiness (unknown direction of change, Zamuda et al. (2013)) over California. All three of these changes impact the environmental covariates in this model. The model results suggest that the south slope trees become severely water limited by the end of the dry season, and thus further water limitation may either limit their growing season, or create conditions that limit their performance. In contrast, on the north slope, the trees do not appear to be water limited. However, it is unclear whether this makes them more resilient to a hotter or drier future. In our interpretation of parameter differences, north-slope trees likely rely on much higher rates of water usage in order to assimilate carbon. If water becomes a limiting resource in the north-slope microclimate in the future, and VPD levels continue to increase, these north-slope trees may be closer to crisis, choosing between cavitation or carbon starvation, than the south-slope trees would be under a more limited growing season (Wang et al., 2020; Grossiord et al., 2020).

More measurements are needed to elucidate specific mechanisms underlying the parameter differences we have found. Measurements of photosynthesis/gas exchange on the leaf level, or chemical analyses of leaf tissues including C:N ratios or isotopic composition, could help shed light on physiological differences in leaves between populations. These measurements were not practical in our study given our lack of canopy access, but more measurements on these trees, or parallel investigations in a greenhouse, could be useful as a future study.

Appendix A Estimation of Direct-Beam Insolation on a Slope

The estimation of direct-beam solar irradiance on horizontal surfaces and slopes is calculated using Python's 'solarradiation' library (Stafford, 2018), which follows the formulation of Duffie and Beckman (1991).

At a time given by day of year n and hour of day $thour$, the incident beam insolation on a horizontal surface S_{flat} at latitude lat (degrees) and 0 degree longitude, is:

$$S_{\text{flat}} = SC \times (1 + 0.033 * \cos(360 * n/365)) * \cos\theta_z, \tag{A1}$$

where

$$\delta = 23.45 \times \sin\left(360\frac{284+n}{365}\right), \tag{A2}$$

$$\omega = (thour - 12)/15 \times d2r, \tag{A3}$$

$$\phi = lat \times d2r, \tag{A4}$$

$$\cos\,\theta_z = \cos\,\phi\,\cos\,\delta\,\cos\,\omega\,+\,\sin\,\phi\,\sin\,\delta \tag{A5}$$

$$\tag{A6}$$

and $SC = 1361$ W/m^2 is the solar constant, and $d2r = \pi/180$ converts degrees to radians. δ is declination; ω is the hour angle; θ_z is the zenith angle.

The ratio R_b between the direct-beam on horizontal and hilly surface with *slope* (in degrees) and *aspect* (clockwise from North in degrees) is:

$$R_b = \frac{\cos\,\theta}{\cos\,\theta_z}, \tag{A7}$$

where

$$\begin{aligned}\cos\theta = {} & \sin\delta\,\sin\phi\,\cos\beta - \sin\delta\,\cos\phi\,\sin\beta\,\cos\gamma + \cos\delta\,\cos\phi\,\cos\beta\,\cos\omega \\ & + \cos\delta\,\sin\phi\,\sin\beta\,\cos\gamma\,\cos\omega + \cos\delta\,\sin\beta\,\sin\gamma\,\sin\omega\end{aligned} \tag{A8}$$

and $\beta = slope \times d2r$, $\gamma = (aspect - 180) \times d2r$ is the azimuth angle of the sloped surface, and θ is the angle between the incident beam and the normal to the sloped surface. The terms S_{N} and S_{S} that appear in the description of the solar model given in Section 2.3 are $S_{\mathrm{flat}} \times R_b$, with R_b tailored to the geometry of each respective hillslope.

Acknowledgments

This project is supported by the DOE Office of Science grants DE-SC0010857 and DE-SC0014080 and NSF Eel River Critical Zone Observatory (EAR-1331940). TEB is also supported by a DOE Office of Science Graduate Student Research Fellowship. Data is available at https://zenodo.org/record/3996308.YG4r7khKhZp, DOI:10.5281/zenodo.3996308. The LiDAR data were provided by the National Center for Airborne Laser Mapping (NCALM). We thank Bill Dietrich and Daniella Rempe for detailed discussions about geology and subsurface moisture at the site; Charlie Koven, Jennifer Johnson and Joe Berry for comments on our sap velocity model interpretations; Colin Bode and David Elvins for support with solar modeling; and Anthony Ambrose, Wendy Baxter, Colin Bode, Michael Diaz, Andrew Levy, Sheila Newbery, Peter Steel, Cecily Tye, Chris Wong, Stephanie Wuerth,

Katelyn Yu, and Lian Zhang for fieldwork support. The authors declare no conflicts of interest.

References

Amitrano, C., Arena, C., Rouphael, Y., De Pascale, S., & De Micco, V. (2019). Vapour pressure deficit: The hidden driver behind plant morphofunctional traits in controlled environments. *Annals of Applied Biology*, *175*(3), 313-325.

Armesto, J. J., & Martinez, J. A. (1978). Relations between vegetation structure and slope aspect in the mediterranean region of chile. *Journal of Ecology*, *66*(3), 881–889.

Asner, G. P., Brodrick, P. G., Anderson, C. B., Vaughn, N., Knapp, D. E., & Martin, R. E. (2016). Progressive forest canopy water loss during the 2012–2015 california drought. *Proceedings of the National Academy of Sciences*, *113*(2), E249–E255. doi: 10.1073/pnas.1523397113

Betancourt, M. (2017). A conceptual introduction to hamiltonian monte carlo. *arXiv preprint arXiv:1701.02434*.

Bilir, T. E. (2020). *Data and software accompanying "slope-aspect induced climate differences influence how water is exchanged between the land and atmosphere".* Zenodo. Retrieved from `https://doi.org/10.5281/zenodo.3996308` doi: 10.5281/zenodo.3996308

Boardman, N. K. (1977). Comparative photosynthesis of sun and shade plants. *Annual review of plant physiology*, *28*(1), 355–377.

Bolton, D. (1980). The computation of equivalent potential temperature. *Monthly weather review*, *108*(7), 1046–1053.

Brooks, J. R., Meinzer, F. C., Coulombe, R., & Gregg, J. (2002). Hydraulic redistribution of soil water during summer drought in two contrasting pacific northwest coniferous forests. *Tree physiology*, *22*(15-16), 1107–1117.

Brooks, J. R., Meinzer, F. C., Warren, J. M., Domec, J.-C., & Coulombe, R. (2006). Hydraulic redistribution in a douglas-fir forest: lessons from system manipulations. *Plant, Cell & Environment*, *29*(1), 138–150.

Chapin, F. S., Bloom, A. J., Field, C. B., & Waring, R. H. (1987). Plant responses to multiple environmental factors. *BioScience*, *37*(1), 49–57.

De Frenne, P., Rodríguez-Sánchez, F., Coomes, D. A., Baeten, L., Verstraeten, G.,

Vellend, M., ... Verheyen, K. (2013). Microclimate moderates plant responses to macroclimate warming. *Proceedings of the National Academy of Sciences*, *110*(46), 18561–18565. Retrieved from https://www.pnas.org/content/110/46/18561 doi: 10.1073/pnas.1311190110

De Frenne, P., Zellweger, F., Rodríguez-Sánchez, F., Scheffers, B. R., Hylander, K., Luoto, M., ... Lenoir, J. (2019). Global buffering of temperatures under forest canopies. *Nature Ecology & Evolution*, *3*, 744-749. Retrieved from https://doi.org/10.1038/s41559-019-0842-1 doi: 10.1038/s41559-019-0842-1

Duffie, J. A., & Beckman, W. A. (1991). *Solar engineering of thermal processes john wiley & sons*. John Willey & Sons.

Feddes, R., Kowalik, P., & Zaradny, H. (1978). *Simulation of field water use and crop yield john wiley and sons*. New York, NY: John Wiley and Sons.

Fettig, C. J., Mortenson, L. A., Bulaon, B. M., & Foulk, P. B. (2019). Tree mortality following drought in the central and southern sierra nevada, california, u.s. *Forest Ecology and Management*, *432*, 164 - 178. doi: https://doi.org/10.1016/j.foreco.2018.09.006

Gimenez, B. O., Jardine, K. J., Higuchi, N., Negrón-Juárez, R. I., Sampaio-Filho, I. d. J., Cobello, L. O., ... Chambers, J. Q. (2019). Species-specific shifts in diurnal sap velocity dynamics and hysteretic behavior of ecophysiological variables during the 2015–2016 el niño event in the amazon forest. *Frontiers in Plant Science*, *10*, 830. Retrieved from https://www.frontiersin.org/article/10.3389/fpls.2019.00830 doi: 10.3389/fpls.2019.00830

Gorelick, N., Hancher, M., Dixon, M., Ilyushchenko, S., Thau, D., & Moore, R. (2017). Google earth engine: Planetary-scale geospatial analysis for everyone. *Remote Sensing of Environment*. Retrieved from https://doi.org/10.1016/j.rse.2017.06.031 doi: 10.1016/j.rse.2017.06.031

Granier, A. (1985). Une nouvelle méthode pour la mesure du flux de sève brute dans le tronc des arbres. In *Annales des sciences forestières* (Vol. 42, pp. 193–200).

Granier, A. (1987). Evaluation of transpiration in a douglas-fir stand by means of sap flow measurements. *Tree physiology*, *3*(4), 309–320.

Grossiord, C., Buckley, T. N., Cernusak, L. A., Novick, K. A., Poulter, B., Siegwolf, R. T. W., ... McDowell, N. G. (2020). Plant responses to rising vapor

pressure deficit. *New Phytologist*, *226*(6), 1550–1566.

Harrison, J. L., Reinmann, A. B., Maloney, A. S., Phillips, N., Juice, S. M., Webster, A. J., & Templer, P. H. (2020). Transpiration of dominant tree species varies in response to projected changes in climate: Implications for composition and water balance of temperate forest ecosystems. *Ecosystems*, 1–16.

Hassler, S. K., Weiler, M., & Blume, T. (2018). Tree-, stand- and site-specific controls on landscape-scale patterns of transpiration. *Hydrology and Earth System Sciences*, *22*(1), 13–30. doi: 10.5194/hess-22-13-2018

Hoffman, M. D., & Gelman, A. (2014). The no-u-turn sampler: adaptively setting path lengths in hamiltonian monte carlo. *Journal of Machine Learning Research*, *15*(1), 1593–1623.

Holland, P. G., & Steyn, D. G. (1975). Vegetational responses to latitudinal variations in slope angle and aspect. *Journal of Biogeography*, *2*(3), 179–183.

Jarvis, P. G. (1976). The interpretation of the variations in leaf water potential and stomatal conductance found in canopies in the field. *Philosophical Transactions of the Royal Society of London. Series B, Biological Sciences*, *273*(927), 593–610. Retrieved from `http://www.jstor.org/stable/2417554`

Jasechko, S., Sharp, Z. D., Gibson, J. J., Birks, S. J., Yi, Y., & Fawcett, P. J. (2013). Terrestrial water fluxes dominated by transpiration. *Nature*, *496*(7445), 347–350.

Knapp, A., & Smith, W. (1987). Stomatal and photosynthetic responses during sun/shade transitions in subalpine plants: influence on water use efficiency. *Oecologia*, *74*(1), 62–67.

Knapp, A. K., & Smith, W. K. (1990). Stomatal and photosynthetic responses to variable sunlight. *Physiologia Plantarum*, *78*(1), 160–165.

Kumagai, T., Aoki, S., Shimizu, T., & Otsuki, K. (2007, 02). Sap flow estimates of stand transpiration at two slope positions in a Japanese cedar forest watershed. *Tree Physiology*, *27*(2), 161-168.

Larcher, W. (1995). *Physiological plant ecology, 3rd edition.* Springer-Verlag.

Lee, J.-H., Biging, G. S., & Fisher, J. B. (2016). An individual tree-based automated registration of aerial images to lidar data in a forested area. *Photogrammetric Engineering & Remote Sensing*, *82*(9), 699-710. Retrieved from `https://www.ingentaconnect.com/content/asprs/pers/2016/00000082/`

00000009/art00017 doi: doi:10.14358/PERS.82.9.699

Link, P., Simonin, K., Maness, H., Oshun, J., Dawson, T., & Fung, I. (2014). Species differences in the seasonality of evergreen tree transpiration in a mediterranean climate: Analysis of multiyear, half-hourly sap flow observations. *Water Resources Research*, *50*(3), 1869–1894.

Lohammar, T., Larsson, S., Linder, S., & Falk, S. O. (1980). Fast: Simulation models of gaseous exchange in scots pine. *Ecological Bulletins*(32), 505–523. Retrieved from http://www.jstor.org/stable/20112831

Mencuccini, M., Manzoni, S., & Christoffersen, B. (2019). Modelling water fluxes in plants: from tissues to biosphere. *New Phytologist*, *222*(3), 1207–1222.

Metzen, D., Sheridan, G. J., Benyon, R. G., Bolstad, P. V., Griebel, A., & Lane, P. N. (2019). Spatio-temporal transpiration patterns reflect vegetation structure in complex upland terrain. *Science of The Total Environment*, *694*. doi: https://doi.org/10.1016/j.scitotenv.2019.07.357

Oshun, J. (2016). *The isotopic evolution of a raindrop through the critical zone* (Unpublished doctoral dissertation). UC Berkeley.

Pappas, C., Fatichi, S., & Burlando, P. (2016). Modeling terrestrial carbon and water dynamics across climatic gradients: does plant trait diversity matter? *New Phytologist*, *209*(1), 137-151. doi: https://doi.org/10.1111/nph.13590

Pearcy, R. W. (1998). Acclimation to sun and shade. In A. S. Raghavendra (Ed.), *Photosynthesis: A comprehensive treatise* (p. 250-263). Cambridge: Cambridge University Press.

Rempe, D. M. (2021). *Eel river czo soil properties.* Hydroshare. Retrieved from https://doi.org/10.4211/hs.137b111c10a84946a184422f74fda8dd doi: 10.4211/hs.137b111c10a84946a184422f74fda8dd

Rempe, D. M., & Dietrich, W. E. (2018). Direct observations of rock moisture, a hidden component of the hydrologic cycle. *Proceedings of the National Academy of Sciences*, *115*(11), 2664–2669.

Renner, M., Hassler, S. K., Blume, T., Weiler, M., Hildebrandt, A., Guderle, M., ... Kleidon, A. (2016). Dominant controls of transpiration along a hillslope transect inferred from ecohydrological measurements and thermodynamic limits. *Hydrology and Earth System Sciences*, *20*(5), 2063–2083. doi: 10.5194/hess-20-2063-2016

Romero-Lankao, P., Smith, J., Davidson, D., Diffenbaugh, N., Kinney, P., Kirshen, P., ... Villers Ruiz, L. (2014). North america. In V. Barros et al. (Eds.), *Climate change 2014: Impacts, adaptation, and vulnerability. part b: Regional aspects.* (p. 1439-1498). Cambridge, United Kingdom and New York, NY, USA: Cambridge University Press.

Salvatier, J., Wiecki, T. V., & Fonnesbeck, C. (2016). Probabilistic programming in python using pymc3. *PeerJ Computer Science*, *2*, e55.

Schimper, A. F. W. (1903). *Plant-geography upon a physiological basis.* (P. Groom & I. B. Balfour, Eds. & W. R. Fisher, Trans.). Oxford, United Kingdom: Oxford Clarendon Press.

Stafford, B. (2018, September). *pysolar.* Zenodo. Retrieved from `https://doi.org/10.5281/zenodo.1461066` doi: 10.5281/zenodo.1461066

Stokes, V. J., Morecroft, M. D., & Morison, J. I. (2010). Comparison of leaf water use efficiency of oak and sycamore in the canopy over two growing seasons. *Trees*, *24*(2), 297–306.

USDA. (2008). *CALVEG zones and alliances: vegetation descriptions* (Tech. Rep.). Retrieved from `http://www.fs.usda.gov/Internet/FSE_DOCUMENTS/fsbdev3_046448.pdf`

Vrettas, M. D., & Fung, I. Y. (2017). Sensitivity of transpiration to subsurface properties: Exploration with a 1-d model. *Journal of Advances in Modeling Earth Systems*, *9*(2), 1030–1045.

Wang, Y., Sperry, J. S., Anderegg, W. R., Venturas, M. D., & Trugman, A. T. (2020). A theoretical and empirical assessment of stomatal optimization modeling. *New Phytologist*.

Ward, E. J., Domec, J.-C., King, J., Sun, G., McNulty, S., & Noormets, A. (2017). Tracc: an open source software for processing sap flux data from thermal dissipation probes. *Trees*, *31*(5), 1737–1742.

Waring, R. H., & Landsberg, J. J. (2011, 03). Generalizing plant–water relations to landscapes. *Journal of Plant Ecology*, *4*(1-2), 101-113. Retrieved from `https://doi.org/10.1093/jpe/rtq041` doi: 10.1093/jpe/rtq041

Young, D., & Smith, W. (1979). Influence of sunflecks on the temperature and water relations of two subalpine understory congeners. *Oecologia*, *43*(2), 195–205.

Young, D. J. N., Stevens, J. T., Earles, J. M., Moore, J., Ellis, A., Jirka, A. L., &

Latimer, A. M. (2017). Long-term climate and competition explain forest mortality patterns under extreme drought. *Ecology Letters*, *20*(1), 78-86. doi: https://doi.org/10.1111/ele.12711

Zamuda, C., Mignone, B., Bilello, D., Hallett, K., Lee, C., Macknick, J., ... Steinberg, D. (2013). *Us energy sector vulnerabilities to climate change and extreme weather* (Tech. Rep.). Washington DC: Department of Energy.

Zhang, Q., Manzoni, S., Katul, G., Porporato, A., & Yang, D. (2014). The hysteretic evapotranspiration—vapor pressure deficit relation. *Journal of Geophysical Research: Biogeosciences*, *119*(2), 125-140. Retrieved from `https://agupubs.onlinelibrary.wiley.com/doi/abs/10.1002/2013JG002484` doi: 10.1002/2013JG002484